Enabling Long-term Cycling Stability of $Na_3V_2(PO_4)_3$/C *vs.* Hard Carbon Full-cells

Pirmin Stüble,[a,*] Cedric Müller,[a] Julian Klemens,[b] Philip Scharfer,[b] Wilhelm Schabel,[b] Marcel Häringer,[a] Joachim R. Binder,[a] Andreas Hofmann,[a] and Anna Smith[a*]

a: Institute for Applied Materials (IAM)
Karlsruhe Institute of Technology (KIT)
Hermann-von-Helmholtz-Platz 1
76344 Eggenstein-Leopoldshafen (Germany)

b: Thin Film Technology (TFT)
Karlsruhe Institute of Technology (KIT)
Straße am Forum 7
76131 Karlsruhe (Germany)

✉: pirmin.stueble@kit.edu,
anna.smith@kit.edu

Abstract

Sodium-ion batteries are becoming an increasingly important complement to lithium-ion batteries. However, while extensive knowledge on the preparation of Li-ion batteries with excellent cycling behavior exists, studies on applicable long-lasting sodium-ion batteries are still limited. Therefore, this study focuses on the cycling stability of batteries composed of $Na_3V_2(PO_4)_3$/C based cathodes and hard carbon anodes. It is shown that full cells with a decent stability are obtained for ethylene carbonate / propylene carbonate electrolyte and the conducting salt $NaPF_6$. With cathode loadings of 1.2 mAh/cm², after cell formation discharge capacities up to 92.6 mAh/g are obtained, and capacity retentions > 90 % over 1000 charge / discharge cycles at 0.5 C / 0.5 C are observed. It is shown that both, the additive fluoroethylene carbonate and traces of water in the cell, negatively affect the overall discharge capacity and cycling stability and should therefore be avoided. Remarkably, the internal resistances of well-balanced and well-built cells did not increase over 1500 cycles and 5 months of testing, which is a very promising result regarding the possible lifespan of the cells. The initial loss of active sodium in hard carbon remains a major problem, which can only be partially reduced by proper balancing.

1 Introduction

$Na_3V_2(PO_4)_3$ (NVP) is long known to battery research, although, for nearly a decade it was merely considered as a precursor for cathode materials for lithium-ion batteries (LIBs) like e.g. $Li_2NaV_2(PO_4)_3$, which was accessible exclusively through cation exchange reactions.[1] The use as an electrode material for sodium-ion batteries (SIBs) came into focus around 2010[2] and considerable progress was made when it was found that the issue of low electronic conductivity could be addressed by carbon coatings.[3] Common notations indicating the carbon content of such NVP composite material include NVP/C or NVP@C. In 2013, it was finally demonstrated that stable cycling can be achieved when using NVP/C cathode active material together with sodium metal anodes.[4]

NVP itself crystallizes in the so called NaSICON (Na^+ Superlonic Conductor) structure-type in space group $R\bar{3}c$H. Two sodium ions occupying the 18*b* site of NVP can be extracted leading to the formal composition $Na_1V_2(PO_4)_3$. The mobilization of the remaining sodium cation from Wyckoff site 6*b* is not possible within the stability range of common electrolytes[1,5,6] and, to the best our knowledge, a fully de-sodiated state

has not been reported so far. But besides extracting sodium ions, it is also possible to insert additional sodium ions into the crystal structure of NVP. The insertion of a fourth Na^+ ion is observed a ~1.6 V (vs Na/Na^+)[3] and a fifth sodium can be inserted at ~0.3 V (vs. Na/Na^+), leading to the composition $Na_5V(PO_4)_3$.[7] Even higher sodiation states like $Na_6V(PO_4)_3$ have also been reported and discussed.[8]

For practical application in a SIB, however, sodiation levels of $1 \leq x \leq 4$ in $Na_xV_2(PO_4)_3$ are of particular importance. When functioning as a cathode, common voltage windows like 2.3 to 3.9 V,[9] cover V^{III}/V^{IV} redox activity with the formal reaction $Na_3V_2^{III/III}(PO_4)_3 \rightleftharpoons Na_2V_2^{III/IV}(PO_4)_3 \rightleftharpoons NaV_2^{IV}(PO_4)_3$ at roughly 3.4 V (*vs.* Na/Na^+), corresponding to a specific capacity of 116.6 mAh/g. When cycling against Na metal anodes, the capacity can easily be increased by reducing the lower voltage limit, e.g. to 1.2 V. During discharge, the fourth Na^+-ion is inserted according to $Na_3V_2^{III/III}(PO_4)_3 + Na^+ + e^- \rightleftharpoons Na_4V_2^{II/III}(PO_4)_3$, leading to a partial reduction of vanadium to V(II) and an increase of the capacity to 174.9 mAh/g (based on the molar mass of N_3VP). However, while a fourth Na^+-ion leads to a capacity increase by 50 %, the energy density increases by only about 22 % due to the lower voltage of the V(II)/V(III) redox step. Additionally, the insertion of the fourth Na^+ ion occurs along with an additional two phase reaction,[3,10] which can lead to accelerated degradation of the NVP active material.[9]

It is a peculiarity of SIBs, that graphite based anodes, that are state of the art electrodes in commercial LIBs, cannot be used due to lack of solvent-free intercalation ability of sodium between graphite layers.[11] Hard Carbon (HC) is commonly used instead, which is challenging and advantageous at the same time. On the positive side, compared to graphite, HC has an abundant choice of precursors and a good perspective for the reduction of production cost and environmental impact.[12] HC is therefore regarded as the most promising candidate for anode materials in commercial SIBs.[12,13] One the negative side, however, the initial capacity loss of HC during battery formation is still higher than for graphite-based anodes in state of the art LIB-systems.[14] As a consequence, proper balancing of the capacity ratio of negative to positive electrode (N/P), is crucial. The areal capacity of the HC anode should slightly exceed the capacity of the cathode in order to avoid sodium plating and dendrite formation. Simultaneously, the capacity of the anode should not be significantly higher or overbalanced, as this leads to even higher losses of electrochemically active sodium from the cathode during cell formation and thus to a loss of capacity and with that energy density of the battery cell. To address the issue of irreversible sodium loss, promising pre-sodiation strategies for SIBs with HC anodes have recently been developed, e.g. by using Na-biphenyl,[10] $Na_2C_2O_4$,[15] or $Na_4C_4O_4$.[16] However, to the best of our knowledge, such pre-sodiation strategies have so far only been implemented on a laboratory scale.

With vanadium, NVP contains a rare and expensive transition metal, which currently reduces the perspective of large-scale application.[17] However, the possibility of recovering and reusing vanadium to a large extent, as required by current regulatory frameworks for batteries,[18] could increase the attractiveness and sustainability of the system. Another prerequisite to compensate for these disadvantages, would be the possibility to build exceptionally stable and long-lasting cells, to which this paper is meant to contribute. While there are already a number of studies with very promising cycling stabilities for symmetric NVP/C *vs.* NVP/C cells or NVP/C *vs.* Li half-cells,[4,19,20] where 10000 cycles and more were realized, the number of studies on NVP/C *vs.* HC full-cells is quite limited and the cell degradation remains a major obstacle.[5,21] Figure 1 shows the capacity retention of NVP/C *vs.* HC full-cells against the number of cycles reported in literature. More detailed information on the individual studies is given in Table S1. It becomes obvious that numerous studies report quite different lifetimes for NVP/C *vs.* HC cells, which may be largely due to different electrolytes, loadings and C-rates, or possibly also due to external factors such as cell assembly, which - especially in the case of coin cells - has an enormous influence on the long term cycling stability.[22] The cause of the capacity decay in full-cells has been investigated previously.[10] Herein, loss of active sodium to the solid electrolyte interface (SEI) is reported

to lead to a decrease of the overall capacity of the NVP/C *vs.* HC cells. The same study reports an almost full recovery of the NVP/C capacity when cycled against fresh sodium. This mechanism for capacity loss is by no means new or unusual, but is also well documented for LIBs, as recently shown in a study on long-term stable $LiNi_{0.5}Mn_{1.5}O_4$ *vs.* graphite full-cells.[23] Although we were not yet able to completely prevent capacity loss, with this study, we would like to show how NVP/C *vs.* HC full-cells with a very promising cycling stability can be prepared. These results may be considered as a starting point for further improvement, e.g. through more adequate electrolytes, the use of additives, pre-sodiation strategies and by using more appropriate long-term stable cell formats, such as pouch cells.

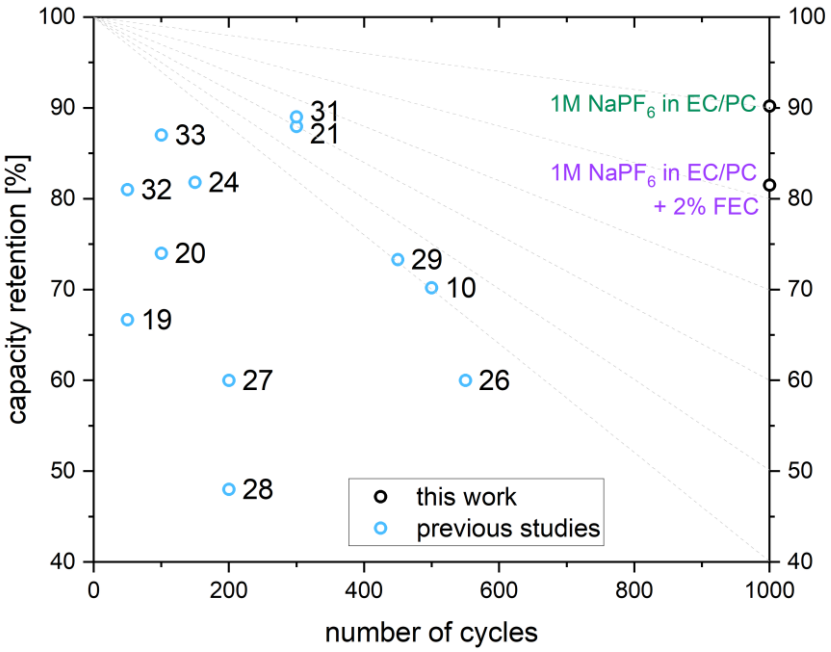

Figure 1: Cycling stability of NVP/C vs. HC full-cells in previously published studies,[10,19–21,24–33] compared to the present work. Further experimental information (if available) are summarized in Table S1.

Unfortunately, it becomes obvious that data reported in the literature is almost impossible to compare. We have tried to extract information on electrode formulation, loading, balancing factor, ratio of electrolyte to NVP. However, most publication lack in one or multiple information on key data. A table of cell information that was possible to extract from experimental data is shown in Table S1.

2 Experimental

2.1 Preparation of the NVP/C Composite Material

Similar to previous works,[19] the NVP/C composites were synthesized via a two-step spray-drying process. Na_2CO_3, $NH_4H_2PO_4$, NH_4VO_3 and β-lactose in a molar ratio of 1:2:1.3:0.7 were dissolved in water at 73 °C and spray dried in a MobileMinor spray drier (GEA) with an inlet and outlet temperature of 210 °C and 112 °C, respectively. In order to decompose the precursor, the powder obtained was calcined in a CWF 63 furnace (Carbolite Gero). At a rate of 60 K/h, the precursor was heated to 450 °C and held for 2 h. Subsequently, with a rate of 180 K/h, the furnace was further heated 850 °C, held for 5 h and then cooled to room temperature at a cooling rate set to 300 K/h. Below approximately 500 °C actual cooling rates were slower due to the lack of active cooling. The whole thermal process was carried out under argon atmosphere. The resulting pre-calcined powder was crushed in a mortar grinder and then ground in a ball mill for with ZrO_2 grinding balls (⌀: 0.2 mm). Before the second spray driying process with the same inlet

and outlet temperatures, a solution of polyacrylic acid (M_n = 1800, 10.1 g/l) and polyethyleglycol (M_n = 400, 0.9 g/l) was added. The powder obtained was calcined again in the same furnace, which was heated to 800 °C with 180 K/h and held for 5 h in an Ar-H atmosphere (97:3 wt%) with continuous gas flow. The resulting NVP/C composite was crushed with a mortar grinder and sieved with a 32 µm sieve. By means of mercury intrusion porosimetry, the porosity inside the NVP/C granules was determined to be 36.8 % at a major pore width of 15 nm. The evaluation of nitrogen adsorption isotherms according to the Brunauer Emmett Teller theory yielded a specific surface area of of 95.5 m^2/g. The carbon content was determined to be 9.8 % by means of elemental analysis.

2.2 Electrode Preparation

The electrodes investigated originate from large-scale processing developed in cooperation with several institutes of KIT.[34–36] A detailed description focusing on NVP/C processing was recently provided by Klemens *et al.*[37] and here we briefly summarize the process. The slurry for NVP/C cathodes was mixed in a dissolver (Dispermat SN-10, VMA Getzmann), where carbon black (C65, C-Nergy) and graphite (KS6L, Timical-Imerys), a PVDF (Solef 5130, Solvay) binder-solvent solution with 7.5 wt.% and about 50 % of the required amount of NMP were dispersed. The NVP/C composite material and remaining NMP were added to the dispersed PVDF/NMP and conductive additive slurry to adjust the solid content to 50 wt.%. Vacuum was applied to remove existing gases from the slurry. The slurries for the HC electrodes were prepared accordingly, but in an aqueous process. The conductive additive Super C65 (Imerys) and a MAC500LC (Nippon Paper) carboxymethyl cellulose (CMC) binder-solvent solution with 2 wt.% were dispersed. HC (Kuranode Type II, 9 µm, Kuraray) and additional water were added to adjust the solid content to 43 wt.%. In a last mixing step, styrene-butadiene rubber (SBR, Zeon Europe) was added. The electrode coating and drying was carried out under quasi-isothermal drying conditions as a discontinuous process likewise described by Klemens et al.[34–37] The slurries were applied to an aluminum current collector by a doctor blade (ZUA 2000.60, Zehntner) and dried by an impingement dryer and temperature controlled heating plates, resulting in drying rates of 0.75 g m^{-2} s^{-1} in both cases. After drying, the electrodes were calendered at 50 °C. The composition of the cathode and anode results as 90.5 wt.% NVP/C, 3 wt.% C65, 2 wt.% KS6L and 4.5 wt.% PVDF and 93 wt.% HC, 1.4 wt.% C65, 1.87 wt.% CMC, 3.73wt.% SBR, respectively.

2.3 Electrolyte Preparation:

Electrolytes A and A+FEC were prepared in an argon filled glovebox (MBraun) with oxygen and water levels below 0.5 ppm. Ethylene carbonate (EC, Gotion, 99.9 %) and propylene carbonate (PC, Gotion, 99.9 %) were used as electrolyte solvents in a mass ratio of 1:1. The conducting salt $NaPF_6$ (1 M, CHEMFISH TOKYO CO.,LTD, 99.9 %) and, if necessary, fluoroethylene carbonate (FEC, Gotion, 99.9 %) were added in a plastic 10 mL volumetric flask for precise preparation of 1 mol/L conducting salt concentration. The electrolytes were then stored in 10 mL aluminum vials due to the incompatibility of $NaPF_6$ and FEC with glass surfaces.

Electrolyte B was prepared analogously in in a different argon filled Glovebox (O_2 < 0.1 ppm, H_2O < 0.1 ppm). EC (Sigma Aldrich, 99%) was similarly mixed with PC (Sigma Aldrich, 99.7%) in a mass ratio of 1:1 and a 1M $NaPF_6$ (Alfa Aesar, 99%) solution was prepared. The water content of electrolytes A and B was determined by means Karl Fischer titration (C30, Mettler Toledo).

2.4 Half Cell Tests

In order to determine capacity of the HC anode and the NVP/C cathode, electrodes were investigated with sodium metal counter and reference electrodes in a three-electrode setup, which was recently presented and discussed in detail by Müller *et al.*[38] Briefly summarized, it enables accurate and reliable determination of active material capacities even for highly loaded electrodes and minimizes errors originating from potential fluctuations, which is crucial especially in the case of HC. The cathodes and

separators (GF/D, Whatman) were dried at 120 °C under vacuum overnight, cell parts and gaskets were dried at 80°C before being transferred into the glovebox. Cells were assembled in a glove box under argon atmosphere (water <0.1 ppm, oxygen <0.1 ppm). Two separators were placed between working electrode and counter electrode, one separator was placed in front of the reference electrode. Before cycling, the cells rested overnight at room temperature. As stated in Table S2, four constant current (CC) charge and discharge cycles at C/20 were then executed in the voltage window of 2.3 to 3.9 V (NVP/C cathode *vs.* sodium reference electrode) and 2 V to 5 mV (HC anode *vs.* sodium reference electrode). Details on the electrodes are given in Section 3.1.

2.5 Full Cell Test

NVP/C and HC electrode disks (both Ø: 16 mm) were punched out and dried overnight under vacuum at 120 °C. NVP/C *vs.* HC full-cells were then assembled as CR2032 coin cells in an argon filled glove box, using Whatman QMA glass fiber separator (Ø: 16.5 mm) and 110 µl of electrolyte and a spacer disk with a thickness of 1 mm. To calculate the precise balancing later on, electrodes were weighted prior to their use. It has recently been shown that the steel grade of coin cell cases can have an enormous impact on the cycle life of alkali-ion batteries cycled *vs.* carbon-based anodes[22] and accordingly, coin cell parts made of S316L steel were chosen. After crimping, the cells were cleaned to remove any electrolyte deposits and possible salt bridges. Before testing, the cells rested for 12 hours at 25.0 °C to allow the electrolyte to soak into the pores of the electrodes. Cycling then was executed at the same temperature within a climate chamber. All cell tests were performed within the voltage window of 2.3 to 3.9 V. For cell formation, four full cycles with charge and discharge rates of C/20 were completed (cf. Table S2). After the 4th formation cycle, the cells were charged to 3.5 V to avoid a pause in the discharged state. A rate capability test only was performed with some selected cells. As listed in Table S3, the charge rate was kept constant at 0.5 C and each two cycles with discharge rates of 0.5 C, 1C, 2C, 3C, 4C and 5C were passed. In order to verify that no test related damage was dealt, two more test cycles with a discharge rate of 0.5C were added. To investigate the long term cycling stability, for all cells a combined test protocol containing check-up cycles, after each 100 charge-discharge cycles, with direct current internal resistance (RiDC) measurements at different states of charge (SOC) was used. Herein, the cells were charged and discharged at 0.1 C. The discharge capacity obtained was used to calculate the capacities corresponding to a SOC of 10%, 30%, 50%, 70% and 90%, which then were used as measuring points for the RiDC test in the subsequent charging cycle. For the latter, a 20 second pulse with a C-rate of 1C was applied. In order not to falsify the subsequent measurements, the discharged capacity during the RiDC pulse was compensated. Then the cell again was discharged with 0.5C. After these check-up cycles, 100 charge discharge cycles with a constant current constant voltage (CCCV) charging step at 0.5 C (with CV phase until 0.05C) and CC discharge step at 0.5 C were executed. Hereafter, new check-up cycles and the next 100 charge discharge cycles followed, resulting in total test times of roughly 3 to 6 months for 1500 cycles.

2.6 Statistical Analysis

The average loadings of the electrodes were determined based on the weight of 16, 11 and 7 individual electrode discs (Ø = 16 mm) for NVP/C, HC-1 and HC-2, respectively, see Table1. The electrode thicknesses before and after calendering were determined by 4 to 6 single point measurements. The coin cell tests were verified using two identically prepared cells. In case of cells 1-3, 4 and 5 (Table3), the variation between both cell tests was less than 4% and the better performing cell is shown. In the case of cell 4 (overbalancing of the anode + FEC), the second cell failed after some days, so that only a single and therefore less reliable data set is available. This, however is pointed out again in the discussion below.

3 Results and Discussion

3.1 Electrode and Electrolyte Properties

General properties of the NVP/C cathode (NVP-1) and the two differently loaded HC anodes (HC-1 and HC-2) investigated are listed in Table 1. The overall NVP-content in the cathode is 81.6 wt.% resulting from the NVP/C content in the cathode layer (90.5 wt.%) and the NVP content of the NVP/C composite material (90.2 wt.%). Accordingly the average active material loading of the cathode, i.e. the loading of pure NVP, was determined to be 11.1(4) mg/cm² which corresponds to an areal capacity of 1.23(3) mAh/cm², when assuming a specific capacity of 111.3 mAh/g for pure NVP (details see below). The two anodes HC-1 and HC-2 contain 93 wt.% of the HC active material, for which the specific capacity was determined to be 335 mAh/cm².[38] Accordingly, the average HC loadings were determined to be 4.2(2) and 7.0(2) mg/cm² corresponding to areal capacities of 1.53(5) and 2.35(6) mAh/cm². In all cells investigated, the HC anodes were overbalanced compared to NVP and no evidence of Na-plating was found during the investigation. Based on the areal capacities mentioned before, and the circumstance that electrode discs with the same diameter (16 mm) were used, the balancing of the NVP-1 cathode vs. the HC-1 anode is roughly 1 : 1.24, while NVP-1 vs. HC-2 yields a balancing of 1 : 1.91. However, electrode masses and the resulting balancing was determined for each cell individually and the corresponding values are listed in Table 3.

Table 1: General properties of the electrodes investigated. Mean values and standard deviations (in brackets) were calculated based on 16, 11 and 7 electrode discs (⌀ = 16 mm) for NVP, HC-1 and HC-2, respectively. Specific capacities were determined in half-cell configuration using sodium anodes. Electrode thicknesses were calculated before / after calendering based on 4-6 single point measurements.

Label	Active Material (AM)		Electrode Properties			
	Type	Specific capacity	AM content	AM loading	Areal Capacity	Electrode Thickness
		[mAh/g]	[wt.%]	[mg/cm²]	[mAh/cm²]	[µm]
NVP-1	$Na_3V_2(PO_4)_3$	111.3(1)	81.6	11.1(3)	1.23(3)	136(4) / 105(2)
HC-1	Hard Carbon	335.0	93	4.2(2)	1.53(5)	60(5) / 57(2)
HC-2	Hard Carbon	335.0	93	7.0(2)	2.35(6)	96(5) / 84 (2)

An overview of the electrolytes used during this investigation is given Table 2. 1 M $NaPF_6$ in EC/PC and the optional addition of FEC was chosen on the basis of previous studies[39–42] and preliminary screening of the electrolyte stabilities against sodium metal.[38] The water content of electrolyte A was determined to be below 10 ppm by means of Karl-Fischer titration. The water content of the electrolyte A+FEC was not determined separately. However, based on the voltage profiles of the first charging step (cf. Figure 3 and 7), it becomes evident that FEC and trace water have distinguishable effects. Therefore, it is very unlikely that an artifact from trace water introduced with FEC is seen instead of an effect of FEC. Electrolyte B was prepared in another Glovebox, with EC and PC and $NaPF_6$ originating from different suppliers (details see experimental section). The water content of electrolyte B was determined to be 60 ppm. However, as significantly lower values were measured in the corresponding batches of EC and PC, the source of moisture presumably was the conducting salt $NaPF_6$. In case of electrolyte B, the latter may not always have been handled correctly, and was not dried before use.

Table 2: Composition and water content of electrolytes used in full-cells.

Electrolyte	Composition	Water content
A	1M $NaPF_6$ in EC/PC (w/w)	< 10 ppm
A+FEC	1M $NaPF_6$ in EC/PC (w/w)+ 2wt% FEC	not determined, presumably similar to A
B	1M $NaPF_6$ in EC/PC (w/w)	60 ppm

3.2 NVP/C and HC vs. Sodium Half-Cells

The voltage profiles of the formation cycles of a NVP-1 cathode cycled against a sodium metal anode at C/20 are shown in Figure 2a. The discharge capacities of the formation cycles hardly deviate (<0.1 mAh/g) and were determined to be 111.4 mAh/g when referring to the pure NVP active material. The value was confirmed in a second half cell measurement (not shown), where 111.2 mAh/g was found. Therefore, within this work, a specific active material capacity of 111.3(1) mAh/g is assumed for the NVP-1 cathode. Taking into account the carbon content of 9.8 wt% in the NVP/C, a reduced composite material capacity of only 100.4 mAh/g is obtained.

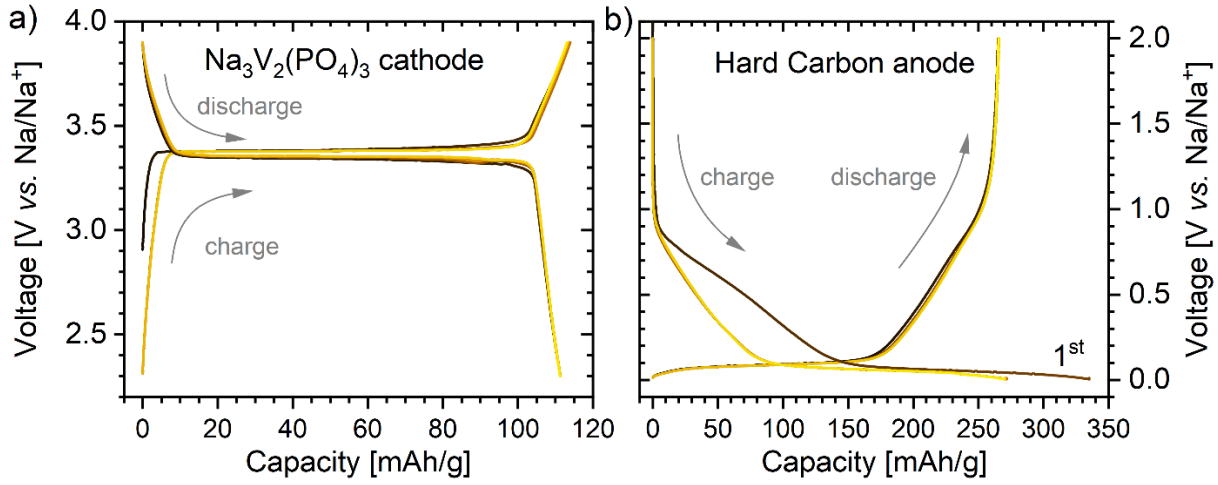

Figure 2: Voltage profiles of the formation cycles of a NVP/C vs. Na half cell (a) and a HC vs. Na half cell (b) at C/20. Lighter colors indicate increasing cycling time.

The capacity of the hard carbon used in anodes HC-1 and HC-2 was determined to be 335.0 mAh/g by means of a three-electrode cell with sodium counter and reference electrode in the voltage range of 5 mV to 2 V (HC vs. reference electrode) at a C-rate of 0.05 C. The value was confirmed in further tests reported by Müller *et al.*[38] Figure 2b, shows the voltage profiles for an electrode prepared in the same way as HC-1 and HC-2, but with a slightly higher loading and an areal capacity of 2.4 mAh/cm². While uniform discharge profiles and a discharge capacity of 269.7 mAh/g are observed, the profile of the first charge cycle of HC deviates significantly from the subsequent charge cycles. This behavior is typical for hard carbon and most recently was attributed mainly to the irreversible binding of sodium on defect sites in HC.[43] For the full cell design and balancing of the cells, the charge capacity of the first cycle is the decisive value. A detailed discussion the capacity of highly loaded HC anodes, investigations of the rate-dependent capacity, and further investigations can be found in a separate work on HC by C. Müller *et al*.[38]

3.3 NVP *vs.* HC Full-cells

3.3.1 Cell Formation

The formation cycles of the NVP/C vs. HC full-cells containing electrolyte A and A+FEC are shown in Figure 3. The charge capacities of the first cycles are in the range of 110.8 to 111.7 mAh/g and, thus, are in very good agreement with the active material capacity of 111.3 mAh/g determined in the half cell. This indicates that even during the first charge cycle, virtually all side reactions involve sodium from the NVP active material. Pure voltage-induced oxidation reactions of the electrolyte, in contrast, do not seem to occur in the voltage window of 2.3 to 3.9 V. In this regard, NVP/C *vs.* HC clearly seems to differ from high voltage (LIB) systems, where additional oxidation reactions occur during SEI formation and the charge capacity of the first cycle significantly exceeds the discharge capacity of the active material, as observed for instance for LNMO *vs.* graphite cells.[23]

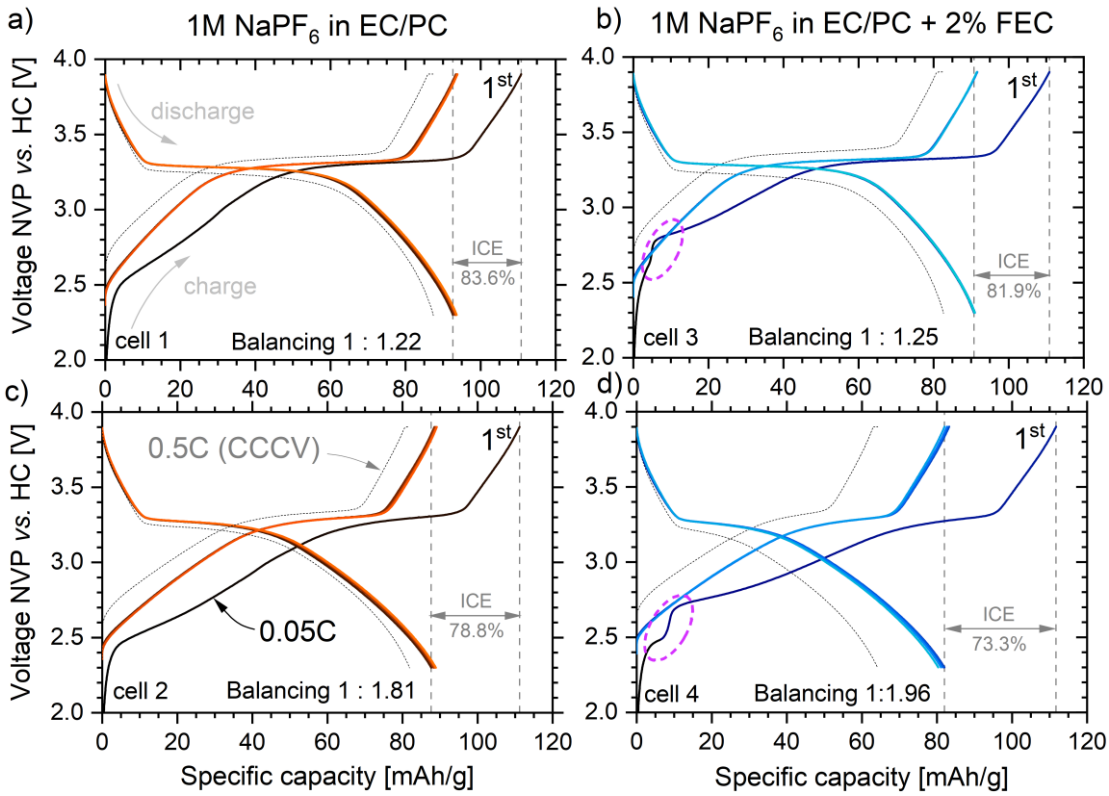

Figure 3: Voltage profiles of the formation cycles of NVP/C vs. HC full-cells with well balanced (a,b) and overbalanced (c,d) anodes at a C-rate of C/20. Electrolyte A without (a,c) and with the additive FEC (b,d) was used. The presumably FEC-specific redox stages in the first charging step are highlighted by pink circles. For comparison, the first full cycle with 0.5 C is represented by the dotted lines. Specific capacities refer to mass of pure NVP.

As discussed above, the discharge capacity of the full-cells with hard carbon anodes are significantly reduced compared to the half-cells as a result to irreversible capacity losses in the first cycle. Based on the current knowledge, this capacity loss can mainly be attributed to defect sites and oxygen functionalities of hard carbon, where sodium is trapped.[43] A peculiarity in the charge profiles of the FEC containing cells is an additional step around 2.5 to 2.7 V, which is encircled in Figure 3 and which indicates slightly different formation processes. For sodium *vs.* hard carbon cells, it was shown that FEC promotes the formation NaF on the surface of hard carbon,[44] which might be a plausible explanation for additional loss of sodium in the FEC containing cells compared to the FEC-free cells.

The individual values of the first cycle discharge capacity during the formation cycles are listed in Table 3 and range from 92.6 to 82.0 mAh/g. During the subsequent formation cycles, there is comparatively little variation in the voltage profiles. In the FEC-free cells, the discharge capacity slightly increases, to 93.3 and 88.9 mAh/g (cells 1 and 3). In the FEC containing, discharge capacities remain almost the same (91.0 mAh/g, cell 2) or slightly decrease to 80.3 mAh/g for cell 4 at the end of the last formation cycle. Hence, from Figure 3 it becomes obvious that the initial loss is influenced by both, NVP *vs.* HC balancing and the use of FEC. The initial coulombic efficiency (ICE) in the cells with the additive FEC is reduced by roughly 2 and 5% when comparing the cell 1 *vs.* 3 and cell 2 *vs.* 4, respectively. For improper balancing the ICE reduction was found to be 5 and 9 % (cell 1 *vs.* 2 and cell 3 *vs.* 4).

For the sake of completeness, the first charge and discharge cycle of the continuous cycling (0.5 CCCV / 0.5C) are also shown in Figure 3 (thin dashed lines). Compared to the formation cycles (0.05 C), in the FEC containing cells, significantly lower capacities are available at 0.5 C than in cells without additive. This could be the result of higher resistance of the SEI, as discussed below, but may also be due to the calendar aging effects associated with FEC.

*Table 3: Overview of the cells investigated in this study. For the calculation of the areal capacities and the resulting cell balancing, specific capacities of 111.3 mAh/g and 335.0 mAh/g for NVP and HC were assumed. Cells 1-4 were built to investigate the impact of FEC and the balancing. Cells 5 and 6 were built 3 months later for an additional investigation of the impact of moisture. Discharge capacities refer to the mass of pure NVP. The results were confirmed by at least one identically built reference cell. *In the case of cell 4, the reference cell test failed, so that only one (less reliable) data set is available.*

Cell	Cathode		Anode		Balancing	Electrolyte	Discharge Capacity	
	type	areal capacity	type	areal capacity	cath. *vs.* anode		0.05 C	0.5 C
		[mAh/cm²]		[mAh/cm²]			[mAh/g]	[mAh/g]
1	NVP-1	1.28	HC-1	1.57	1 : 1.22	A	92.6	87.8
2	NVP-1	1.29	HC-2	2.34	1 : 1.81	A	87.6	82.2
3	NVP-1	1.19	HC-1	1.51	1 : 1.25	A+FEC	90.8	83.0
4*	NVP-1	1.20	HC-2	2.32	1 : 1.96	A+FEC	82.0	64.7
5	NVP-1	1.23	HC-1	1.51	1 : 1.22	A	90.1	87.4
6	NVP-1	1.25	HC-1	1.54	1 : 1.24	B	85.8	80.8

3.3.2 Rate Capability Test

In order to check whether the moderately loaded NVP/C cathodes with 1.2 mAh/cm² can deliver reasonable discharge capacities for rates up to 5 C, after the cell formation, an asymmetric rate capability test was performed in discharge direction with cells 2 and 4. The test protocol is specified in Table S3 and the results are shown in Figure 4. Compared to 0.5 C, a gradual reduction of the discharge capacity with increasing C-rate can be seen. Nevertheless, good discharge capacities are still achieved even at 5 C, where cell 2 and cell 4 deliver 82 % respectively 76 % of the discharge found at 0.5C. This indicates that the loading of the NVP/C electrodes can possibly be increased significantly beyond the 1.2 mAh/cm² investigated herein.

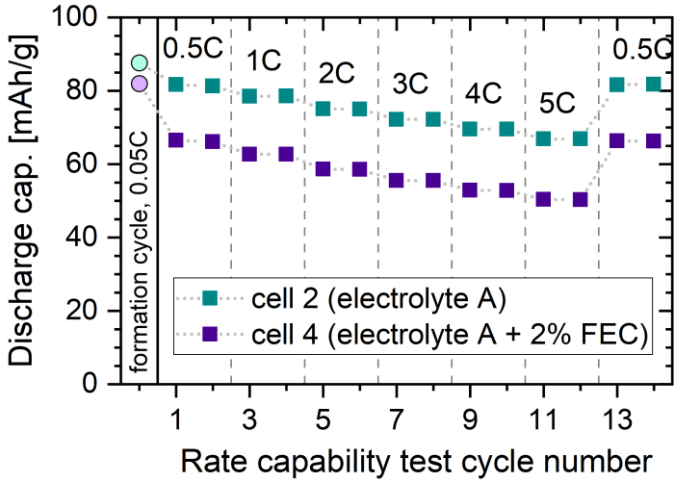

Figure 4: Discharge capacities found for C-rates of 0.5 to 5 C during the rate capability test (CR2032 coin cells, capacities related to the mass of NVP). For comparison, the discharge capacity obtained during cell formation was added on the left (circles). In between, the end of cell formation, cells were charged to 3.5 V and rest for 100 hours before starting the rate capability test.

After formation cycles, the cells were charged to 3.5 V and rested for 100 h at 25 °C before the rate capability test. This pause might be plausible explanation for the high discrepancy of the discharge capacity of formation cycles (0.05 C, shown on the very left of figure 4) compared to the first cycles at 0.5 C in the FEC containing cell, which accounts for 15.4 mAh/g. In the FEC free cell, in contrast, the capacity only is reduced by 5.0 mAh/g from 88.6 (formation, 0.05C) to 81.6 mAh/g at the beginning of the rate capability test (0.5C). While the latter may well be explained by the different C rates, the immense capacity loss of the FEC containing cell suggests ongoing adverse FEC related reactions during storage at 25 °C. Accordingly, the OCV voltage of cell 4 was 3.27 V at the beginning of the rate capability test, which is 5

mV below the 3.34 V measured in cell 2. However, it must be noted that these values interfere with overpotential effects, and that further experiments are necessary to properly understand this calendar aging behavior in detail.

3.3.3 Cycling Stability Test and Internal Resistances

As described in detail in Section 2.5, after cell formation and rate capability tests continuous charge discharge cycles (0.5 CCCV charge, 0.5 C discharge) were carried out with check-up cycles at the beginning and after each 100 cycles (0.1 C charge and discharge). Figure 5 shows the discharge capacities (a,b), as well as the relative discharge capacities, referring to the first cycle of the cycling stability test (c,d). Just like from the formation cycles, it is evident that the balancing directly influences the discharge capacity. An overbalancing of the HC anode leads to reduced starting capacities. The FEC free cells show decent cycling stabilities with similar relative capacity retentions of 89.5 % and 88.6 % after 1000 charge and discharge cycles. The FEC containing cells, in contrast, suffer from accelerated degradation, losing 20 % of their starting capacity after roughly 1060 and 300 charge/discharge cycles, respectively. However, as stated in section 2.6, no comparative data set is available for cell 4 due to early failure of the second cell. Hence, the relatively rapid loss of capacity in this case might have other causes, such as inadequate cell building.

In Figure 5 a and b, the discharge capacities determined in the check-up cycles are depicted as well. It becomes evident that the discrepancy to the discharge capacity at 0.5 C increases both with the overbalancing of the anode and with the additive FEC. This behavior might be due to the higher resistances of the overbalanced HC anodes and the SEIs formed in the FEC containing cells. The voltage profiles of the check-up cycles of cell 1 are depicted in Figure S1 and show now sign of increasing cell polarization. Another notable feature of all cell tests is that the check-up cycles positively influence the capacity of the subsequent cycles. This effect is even more pronounced in the cells with electrolyte B (60 ppm H_2O), and therefore is discussed in the following section 3.3.4.

With the last update, the cell 1 had a remaining capacity of 85.1 % after 1960 cycles and 234 days of testing. All results were achieved in coin cells, which are known to have reduced lifetimes compared to pouch cells.[22] It can therefore be assumed that the degradation can still be significantly reduced by changing the cell format and that an excellent cycling stability should be possible based on NVP/C vs. HC cells with $NaPF_6$ in EC/PC as electrolyte. Likewise, it becomes evident that FEC, which doubtlessly extends the lifetime of NVP *vs.* Na cells,[30] reduces the lifetime of NVP *vs.* HC cells and is therefore not a suitable additive in full-cells.

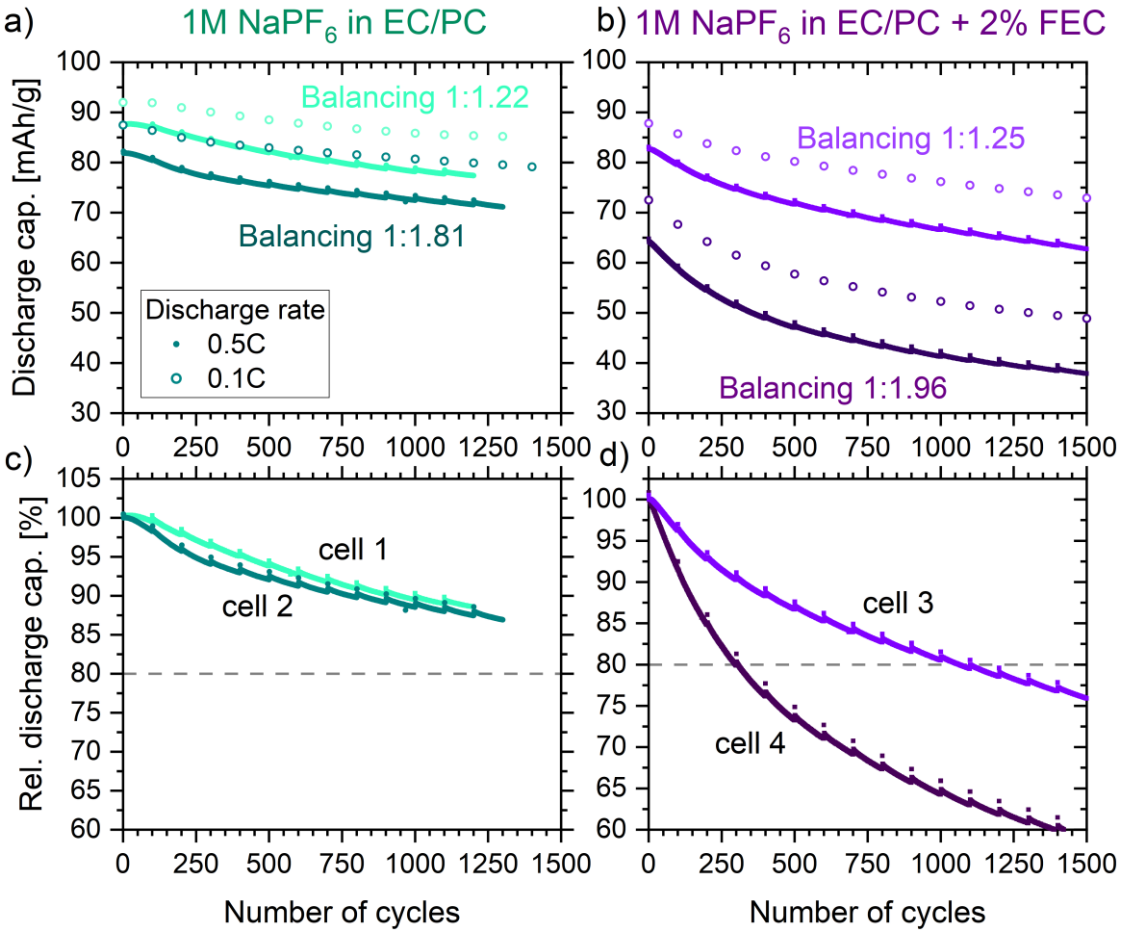

Figure 5: Cycling behavior of NVP/C vs. HC (CR2032 coin cells, capacities related to the mass of NVP) with different electrolytes and different cell balancing at a C rate of 0.5C. a,b) specific discharge capacity c,d) capacity retention, relative to the first discharge cycle at 0.5 C. ---- CELL TESTS STILL RUNNING; DATA WILL BE UPDATED TO AT LEAST 1500 CYCLES FOR ALL CELLS IN THE FINAL VERSION ---

RiDC measurements at different stages of charge were performed at the beginning of the cycling stability test and then each after 100 charge and discharge cycles. The RiDC values varied between 20 and 160 Ω per coin cell. Based on an electrode surface of 2.01 cm², the results were normalized, yielding the specific RiDC values shown in Figure 6. Again, the negative effect of FEC for the full-cells is evident. The cell resistances determined using the RiDC method are about 50 % higher and tend to and increase continuously over time. Remarkably, in the cells where $NaPF_6$ in EC/PC is used as electrolyte, the resistances hardly increase, which is a very encouraging finding with respect to the potential lifetime of the system. Regardless of the additive FEC and number of cycles, in all cells clearly the highest RiDC values were found at a state of charge of 10 %. In contrast, similar and low values were consistently observed for 50 % and 70 % SOC. At 90 % SOC, the resistance increases again noticeably and according to Mohsin *et al.*, the value should become significantly higher again in the fully charged state,[21] which however was not part of our testing protocol.

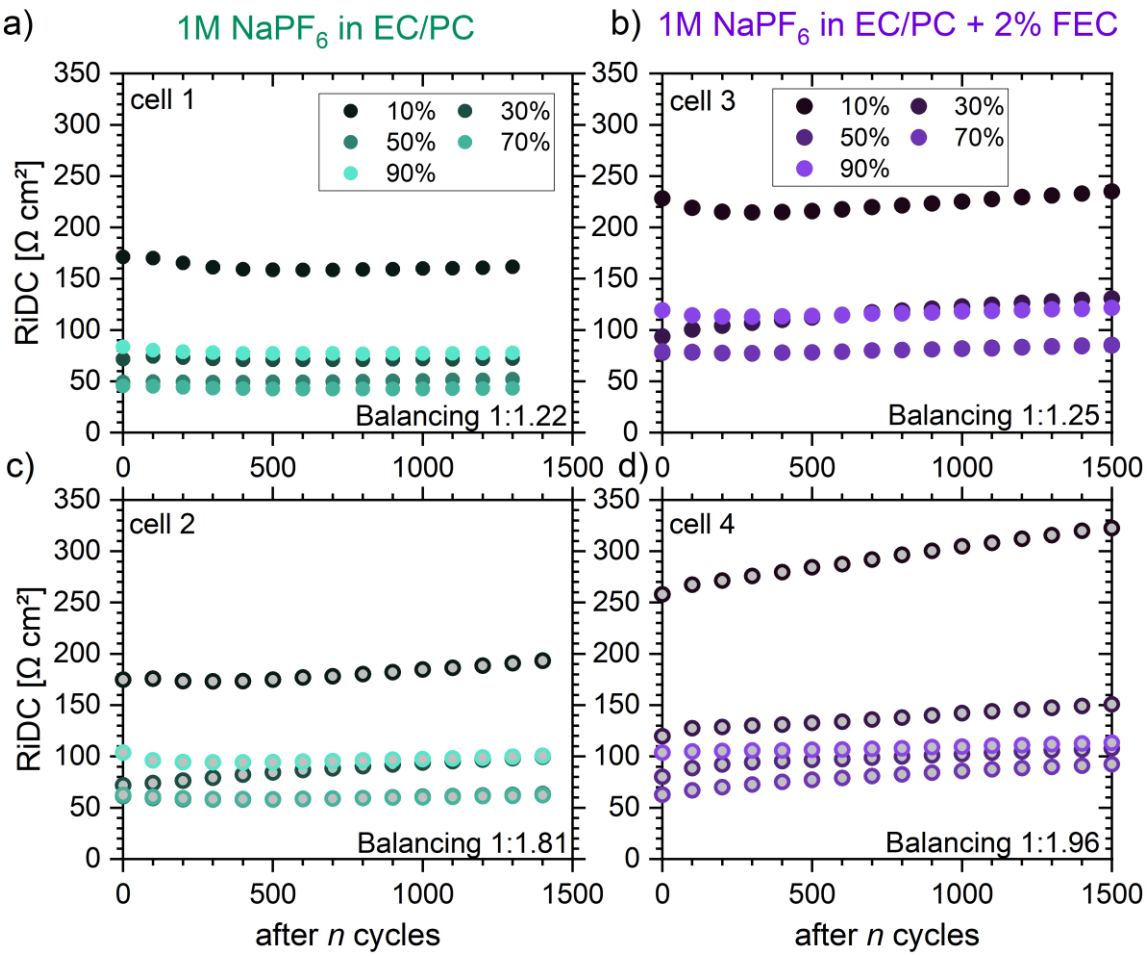

Figure 6: Direct current internal resistance determined from the check-up cycles during the cycling stability test for different states of charge. Both FEC and overbalancing of hard carbon negatively affect the RiDC values. ---- CELL TESTS STILL RUNNING; DATA WILL BE UPDATED TO AT LEAST 1500 CYCLES FOR ALL CELLS ---

Based on the assumption, that the loss of sodium inventory is the predominant cause for capacity loss, formal $Na_{3-x}V_2(PO_4)_3$ compositions after cell formation (20 % Na^+-loss) and of an aged cell (additional 20 % Na^+-loss) were calculated for different stages of charge. Together with the average vanadium oxidation states, the compositions are listed in Table 4. It becomes evident that the compositions at low SOC values are subject to greater changes than those at high SOC values, which is clearly reflected in the variability of the RiDC values observed. Accordingly, in cell 4, which shows the largest increase in RiDC values, over 1500 cycles the resistance at SOC 90 % only increases by 9 Ω cm², while the value for SOC 10 % increases by 65 Ω cm². However, a simple and obvious relationship between SOC, RiDC and phase composition or formal vanadium oxidation states, respectively, cannot be seen. Hence for full and conclusive understanding of the SOC dependency of the RiDC values, further investigations e.g. by means of impedance spectroscopy, seem to be necessary.

Table 4: Formal compositions of the cathode active material $Na_{3-x}V_2(PO_4)_3$ with the corresponding vanadium oxidation states (OS), based on the starting composition $Na_3V_2(PO_4)_3$ and two electrochemically active Na^+ ions ($0 < x < 2$). It is assumed that after formation, roughly 80 % of the active Na^+ ions are still available ($0.4 < x < 2$), and at the end of the lifetime 80 % thereof remain ($0.72 < x < 2$). The Δx values highlight the variation of the composition after formation and at the end of life for different stages of charges.

	after formation (20 % Na^+-loss)			*end of life (80% capacity. ret.)*			
Condition	*x*	Composition	OS(V)	*x*	Composition	OS(V)	Δ*x*
SOC 0%	0.40	$Na_{2.60}V_2(PO_4)_3$	3.20	0.72	$Na_{2.28}V_2(PO_4)_3$	3.36	0.32
SOC 10%	0.56	$Na_{2.44}V_2(PO_4)_3$	3.28	0.84	$Na_{2.16}V_2(PO_4)_3$	3.42	0.28
SOC 30%	0.88	$Na_{2.12}V_2(PO_4)_3$	3.44	1.10	$Na_{1.90}V_2(PO_4)_3$	3.55	0.22
SOC 50%	1.20	$Na_{1.80}V_2(PO_4)_3$	3.60	1.36	$Na_{1.64}V_2(PO_4)_3$	3.68	0.16
SOC 70%	1.52	$Na_{1.48}V_2(PO_4)_3$	3.76	1.62	$Na_{1.38}V_2(PO_4)_3$	3.81	0.10
SOC 90%	1.84	$Na_{1.16}V_2(PO_4)_3$	3.92	1.87	$Na_{1.13}V_2(PO_4)_3$	3.94	0.03
SOC 100%	2.00	$Na_{1.00}V_2(PO_4)_3$	4.00	2.00	$Na_{1.00}V_2(PO_4)_3$	4.00	0.00

Nevertheless, as shown in Figure 6a, in well-balanced, FEC free cells, the RiDC values were almost constant over 1500 cycles and almost 6 months of testing. This is a remarkable and promising result for long-term applications, as it indicates that such cells could potentially be operated for several years and many thousands of cycles. In this respect, the NVP/C *vs.* HC cells reveal a significantly higher stability even when compared to well-established Li-ion cell chemistries such as $LiNi_{0.33}Mn_{0.33}Co_{0.33}O_2$ *vs.* graphite. For the latter, a continuous increase of the RiDC values was consistently observed for very similar cell building parameters and with the same test method.[22]

3.3.4 Impact of Moisture

In order to highlight the impact of moisture in the electrolyte, each two cells were built, in which all parameters were the same except for the use of electrolyte A *vs.* electrolyte B. Although both have the same composition (cf. Table 2), the water content in electrolyte A and B was determined to be < 10 and 60 ppm, respectively. Properties of the individual cells are listed in Table 3. As shown in Figure 7, the traces of water found in electrolyte B seem to significantly affect the first cycle of cell formation. As highlighted in Figure 7b at 3.0 V, an additional step can be seen in the charge profile. The charge capacity of the cell 5 was determined 111.2 mAh/g in the first cycle, which is in perfect agreement with the NVP capacity of 111.3 mAh/g observed in the half-cells (cf. Sections 3.2) and in good agreement with the charge capacities found in cells 1-4 (110.8 – 111.7 mAh/g). In moisture containing cell 6 in contrast, the first charge capacity is slightly increased to 112.3 mAh/g. Even though the excess capacity is small (0.6 mAh/g; 0.3 mAh/g in the second cell), this could be considered an indication that additional side reactions are taking place in the electrolyte in the presence of water. The ICE, which is closely related to the amount of sodium trapped in hard carbon and in the SEI deviates significantly for electrolytes A and B. With the dry electrolyte A, an ICE of 83.4 % is observed, while the cell with the electrolyte B with 60 ppm water only yields 76.4 %. In the subsequent formation cycles, the coulomb efficiencies in the water containing cell 6 remain lower (98.9 – 99.0 %) than in the cell with electrolyte A (99.6 % – 99.8 %).

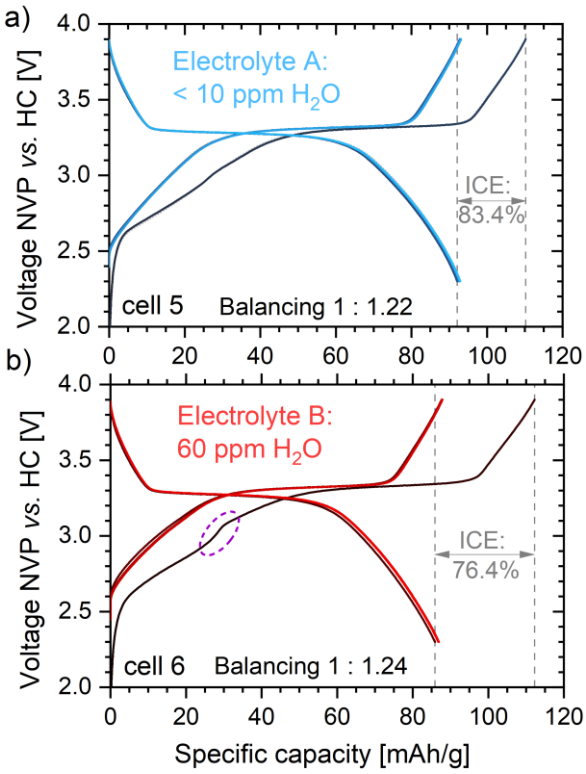

Figure 7: Influence of residual moisture in the electrolyte on voltage profiles of the formation cycles (4 cycles with 0.05 C, the line color becomes lighter with increasing cycle number). The balancing values refer to the capacity of the NVP/C cathode vs. the capacity of the HC anode.

On the basis of the discharge capacity during the cycling stability tests, which are depicted in Figure 8 a and b, the impact of trace water becomes even more obvious. The cells with the rather dry electrolyte show greater capacity retention over the number of cycles than the cells with the water-containing electrolyte, especially over the first 500 cycles. The difference between the discharge capacity in the check-up cycle (0.1C) and the continuous cycling (0.5C) is significantly higher in the case of the water-containing electrolyte, which may be largely due to the internal resistances. The corresponding RiDC values for cells 5 and 6 determined during the cycling stability tests are shown in Figure 8 c and d. In the cells containing water the resistances are clearly higher than those of the cells with the dry electrolyte and even exceed the values observed of the cells containing FEC (see above).

The determination of the water content by means of Karl-Fischer titration and the cell building to study the influence of moisture (cell 5 and 6) was carried out 3 months after the main investigation (cell 1-4). As expected, all cells built with electrolyte A (cell 1, 2 and 5) show a very similar formation behavior (cf. Figure 7a vs. 3a). The RiDC values obtained for cell 1 could likewise be reproduced. In cell 5, slightly higher values were observed, but no significant deviations (cf. Figure 8c *vs.* 6a). The reason for the somewhat greater capacity loss of cell 5 (Figure 8a) compared to cells 1 and 2 (Figure 5a), however, was surprising and cannot be explained straight away. A possible explanation could be that new coin cell sealing gaskets were used. The gaskets did not fit as good as usual and sometimes caused problems when closing the cells. Insufficient sealing of the cell housing is also supported by the observation that the formation cycles appeared normal and the somewhat faster degradation only became noticeable with time.

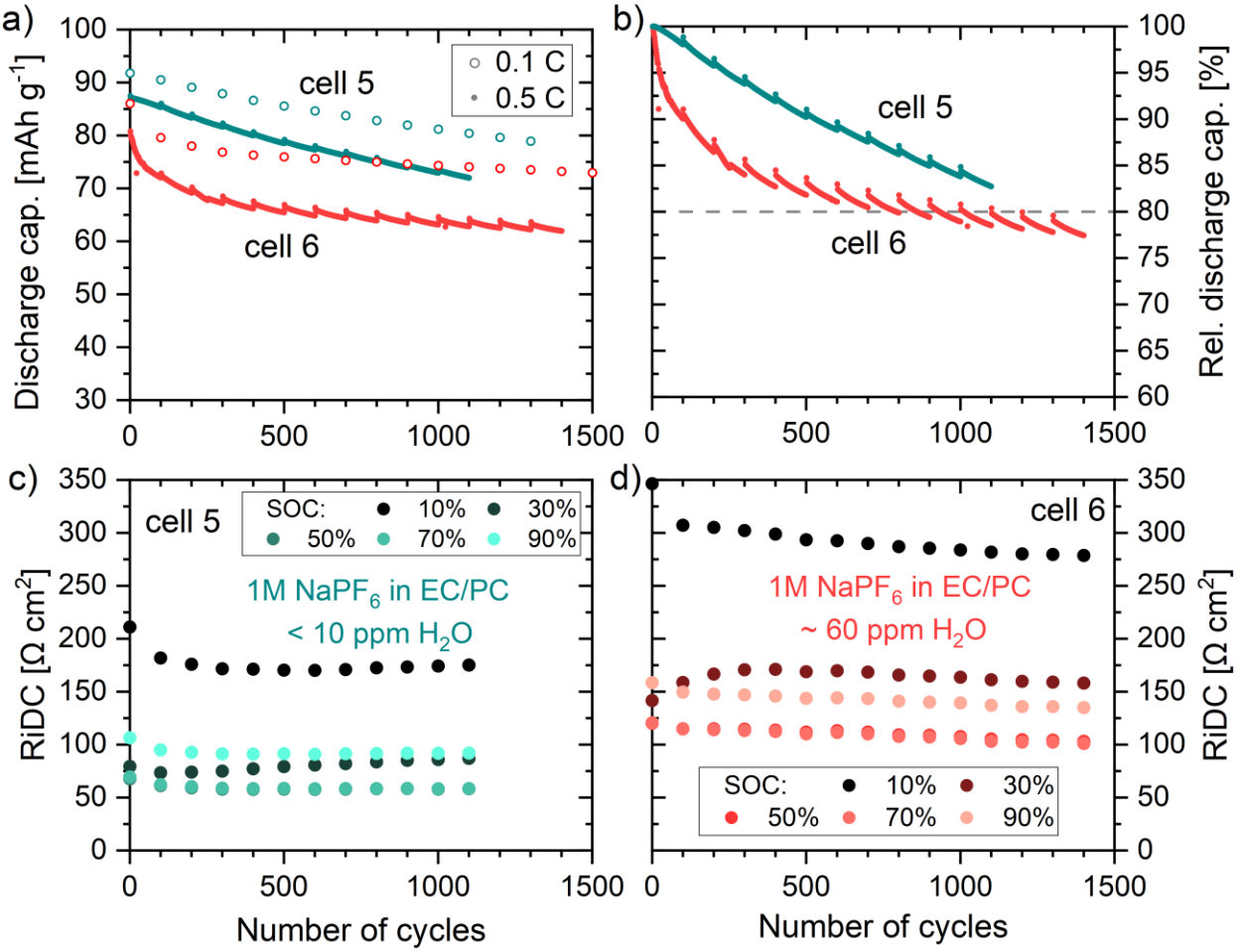

Figure 8: a) Discharge capacity of NVP/C vs. HC full-cells with a well dried electrolyte and an electrolyte with 60 ppm H_2O (capacities related to the mass of NVP). b) Discharge capacity relative to the first discharge cycle at 0.5 C. c,d) Results of the RiDC measurements of the check-up cycles at different stages of charge. ---- CELL TESTS STILL RUNNING; DATA WILL BE UPDATED TO AT LEAST 1500 CYCLES FOR ALL CELLS ---

3.3.5 Pseudo-irreversible Capacity Losses

During this study, it was consistently observed that after the check-up cycles (0.1 C) and RiDC test, the discharge capacity of the subsequent cycles at 0.5 C were noticeably increased for roughly 10 (cells 1), to 50 cycles (cell 6). This becomes particularly evident from the serrated pattern of the 0.5 C discharge capacity shown in Figure 8 a and b, where data from the cell 6 with the moist electrolyte B is shown in red. However, to a weaker extend, all other cells show the same behavior (cf. Figure 5). Hence, it appears that after a slow charging and discharging process, the amount of electrochemically active sodium is increased for the subsequent cycles at the higher C-rate, but then is gradually lost again. The extend of these “pseudo-irreversible” capacity losses in each cell hardly changed over time and amounted to 0.6 mAh/g (cell 1) up to about 1.8 mAh/g (cell 6).

From the 0.5 C profiles in Figure 3 (dotted lines) it becomes also obvious, that a CV phases which were applied in each charge step during the continuous cycling (0.5 C charge with CV step until 0.05 C; 0.5 C discharge), did not make any significant contribution to the overall charge capacity of the NVP/C *vs.* HC cells. Upon a closer inspection, it is therefore likely that the reduced discharge capacities at 0.5 C can explained by the circumstance, that the full-cells were not fully discharged at 0.5 C in the voltage window of 3.9 to 2.3 V. This implies that additional sodium remains pseudo irreversibly trapped in the HC anode during standard cycling. This assumption supported by the fact that the charge capacities in the check-up cycles at 0.1 C, which were performed after 100 cycles at 0.5 C, are reduced compared to the following

discharge capacities at 0.1 C, which can be seen in Figure S1. Accordingly, coulomb efficiencies of ~107 % are observed in these check-up cycles. During standard cycling at 0.5 C in contrast, reduced coulombic efficiencies were observed which then increased until dropping again after the next check-up cycle. An example of this behavior is shown in Figure S2, where a mean coulomb efficiency was fitted over the data points. Regarding the measurement accuracy, however, it must be clearly noted that the test hardware used here reaches its limits, as the absolute CE values and the results for individual cycles are not very reliable and do not allow for further quantitative analysis.
Nevertheless, based on the relative increase in CE values during the standard cycling and the high CE values of the check-up cycles, it seems reasonable to assume that slow discharge processes of the NVP/C *vs.* HC batteries are capable of reactivating some "lost" sodium trapped in the HC anode, which then is lost again over time. It is conceivable that the problem could be reduced by decreasing the lower voltage limit or using a CV phase for the discharge step as well.

4 Conclusions and Outlook

Our study shows that based on NVP/C cathodes and hard carbon anodes, sodium ion batteries with excellent cycling stabilities (> 85 % capacity retention over 1960 cycles) can be realized using EC/PC based electrolyte and the conducting salt $NaPF_6$. Manually built coin cells were investigated, and it can be assumed that with industrial manufacturing technology and in larger cell formats, even significantly better cycling stabilities can be achieved. Based on a rate capability test, it was shown that the electrodes with capacities of ~1.2 mAh/cm² can still provide a considerable discharge capacities even at 5 C (> 75 % compared to 0.5 C), which indicates that the areal capacity of the NVP/C and HC electrodes may still be significantly increased. The balancing of the capacity of the cathode *vs.* the anode hardly affects the cell degradation. However, due to irreversible loss of active sodium within HC anodes, overbalanced anodes lead to even greater losses of the overall cell capacity. Therefore, it is crucial to determine the capacities of the individual electrodes at first and then to balance them as close as possible. Another issue for the NVP/C *vs.* HC cells arises from moisture. It has been shown that even traces of 60 ppm water introduced into the cells via the electrolyte have significant negative effects on the formation, capacity and lifetime. For the full-cells with highest capacity retention investigated, the overbalancing of hard carbon accounted for 30 and 80 %, which led to discharge capacities of 94 mAh and 87 mAh per g NVP, respectively, which is a decent result for NVP/C full-cells. However, these values are still significantly reduced compared to the NVP capacity of 111 mAh/g obtained in half cell configuration. Hence, even with optimal balancing, achieving full-cell capacities of > 100 mAh/g seems to be a great challenge. Therefore, based on the current knowledge, appropriate pre-sodiation strategies seem inevitable and simple and scalable processes need to be developed. The additive FEC, which doubtlessly increases the life-time of NVP/C *vs.* sodium metal half-cells, causes detrimental effects within NVP/C *vs.* HC full-cells. Both, loss of active sodium and accelerated capacity decay are observed. FEC seems to have a negative effect on the SEI formation and causes higher internal resistances, which increase continuously during cell aging. The internal resistances in the cells containing $NaPF_6$ in EC/PC exclusively, in contrast are significantly lower and remain virtually the same even after almost 8 months of testing and nearly 2000 full cycles. This is a highly promising finding, as it indicates that it might be possible to build NVP/C *vs.* HC cells with outstanding cycling stability that can last for years if not for decades, which is decisive for the assessment of the sustainability of the SIB technology.

Author Contributions

Conceptualization: A.S., C.M., P.St. (equal), A.H. (supporting). *Methodology:* A.S., C.M., P.St. (equal). Investigation: P.St. (lead), A.H., C.M., J.K., M.H., (equal.), J.B. (supporting). *Resources*: A.H., A.S., J.B. (equal), P.Sch., W.S. (supp.). *Writing - Original Draft:* P.St. (lead), A.S., C.M., J.B., J.K. (supporting). *Writing - Review & Editing:* A.S., P.St. (equal), A.H., C.M., J.B., J.K., M.H., P.Sch., W.S. (supporting). *Visualization:* P.St. (lead). *Validation:* P.St. (lead), A.S., C.M. (supporting). *Supervision:* A.S., P.St. (equal). *Project administration:* A.S. (lead); *Funding acquisition:* A.S. (lead)

Acknowledgements

We thank Karsten Schmidt for the execution of the Karl-Fischer Titration and Marcus Müller for calendaring the electrodes. Further we would like to thank Steffen Jockisch and Robert Löwe for the support in carrying out and evaluating the cell test. This work contributes to the research performed at CELEST (Center for Electrochemical Energy Storage Ulm-Karlsruhe) and was funded by the German Research Foundation (DFG) under Project ID 390874152 (POLiS Cluster of Excellence, EXC 2154).

5 References

1 B. L. Cushing and J. B. Goodenough, $Li_2NaV_2(PO_4)_3$: A 3.7 V Lithium-Insertion Cathode with the Rhombohedral NASICON Structure, *Journal of Solid State Chemistry*, 2001, **162**, 176–181.

2 L. S. Plashnitsa, E. Kobayashi, Y. Noguchi, S. Okada and J. Yamaki, Performance of NASICON Symmetric Cell with Ionic Liquid Electrolyte, *J. Electrochem. Soc.*, 2010, **157**, A536.

3 Z. Jian, L. Zhao, H. Pan, Y.-S. Hu, H. Li, W. Chen and L. Chen, Carbon coated $Na_3V_2(PO_4)_3$ as novel electrode material for sodium ion batteries, *Electrochemistry Communications*, 2012, **14**, 86–89.

4 K. Saravanan, C. W. Mason, A. Rudola, K. H. Wong and P. Balaya, The First Report on Excellent Cycling Stability and Superior Rate Capability of Na 3 V 2 (PO 4) 3 for Sodium Ion Batteries, *Adv. Energy Mater.*, 2013, **3**, 444–450.

5 X. Zhang, X. Rui, D. Chen, H. Tan, D. Yang, S. Huang and Y. Yu, Na3V2(PO4)3: an advanced cathode for sodium-ion batteries, *Nanoscale*, 2019, **11**, 2556–2576.

6 G. Chen, Q. Huang, T. Wu and L. Lu, Polyanion Sodium Vanadium Phosphate for Next Generation of Sodium-Ion Batteries—A Review, *Adv Funct Materials*, 2020, **30**, 2001289.

7 Z. Jian, Y. Sun and X. Ji, A new low-voltage plateau of Na3V2(PO4)3 as an anode for Na-ion batteries, *Chemical communications (Cambridge, England)*, 2015, **51**, 6381–6383.

8 D. Wang, N. Chen, M. Li, C. Wang, H. Ehrenberg, X. Bie, Y. Wei, G. Chen and F. Du, $Na_3V_2(PO_4)_3$/C composite as the intercalation-type anode material for sodium-ion batteries with superior rate capability and long-cycle life, *J. Mater. Chem. A*, 2015, **3**, 8636–8642.

9 P. L. Mani Kanta, N. L. Priya, P. Oza, M. Venkatesh, S. K. Yadav, B. Das, G. Sundararajan and R. Gopalan, Unusual Case of Higher Cyclic Stability at a Wider Voltage Window in Sodium Vanadium Phosphate, *ACS Appl. Energy Mater.*, 2021, **4**, 12581–12592.

10 Y. Liu, X. Wu, A. Moeez, Z. Peng, Y. Xia, D. Zhao, J. Liu and W. Li, Na-Rich $Na_3V_2(PO4)_3$ Cathodes for Long Cycling Rechargeable Sodium Full Cells, *Advanced Energy Materials*, 2023, **13**, 2203283.

11 M. Goktas, C. Bolli, E. J. Berg, P. Novák, K. Pollok, F. Langenhorst, M. v. Roeder, O. Lenchuk, D. Mollenhauer and P. Adelhelm, Graphite as Cointercalation Electrode for Sodium-Ion Batteries: Electrode Dynamics and the Missing Solid Electrolyte Interphase (SEI), *Adv. Energy Mater.*, 2018, **8**, 1702724.

12 H. Liu, M. Baumann, X. Dou, J. Klemens, L. Schneider, A.-K. Wurba, M. Häringer, P. Scharfer, H. Ehrenberg, W. Schabel, J. Fleischer, N. von der Aßen and M. Weil, Tracing the technology

development and trends of hard carbon anode materials - A market and patent analysis, *Journal of Energy Storage*, 2022, **56**, 105964.
13 F. Xie, Z. Xu, Z. Guo and M.-M. Titirici, Hard carbons for sodium-ion batteries and beyond, *Prog. Energy*, 2020, **2**, 42002.
14 Y. Wan, Y. Liu, D. Chao, W. Li and D. Zhao, Recent advances in hard carbon anodes with high initial Coulombic efficiency for sodium-ion batteries, *Nano Materials Science*, 2022. DOI: 10.1016/j.nanoms.2022.02.001.
15 Y.-B. Niu, Y.-J. Guo, Y.-X. Yin, S.-Y. Zhang, T. Wang, P. Wang, S. Xin and Y.-G. Guo, High-Efficiency Cathode Sodium Compensation for Sodium-Ion Batteries, *Advanced materials (Deerfield Beach, Fla.)*, 2020, **32**, e2001419.
16 D. Shanmukaraj, K. Kretschmer, T. Sahu, W. Bao, T. Rojo, G. Wang and M. Armand, Highly Efficient, Cost Effective, and Safe Sodiation Agent for High-Performance Sodium-Ion Batteries, *ChemSusChem*, 2018, **11**, 3286–3291.
17 M. Baumann, M. Häringer, M. Schmidt, L. Schneider, J. F. Peters, W. Bauer, J. R. Binder and M. Weil, Prospective Sustainability Screening of Sodium-Ion Battery Cathode Materials, *Advanced Energy Materials*, 2022, **12**, 2202636.
18 Vivienne HALLEUX, *New EU regulatory framework for batteries: Setting sustainability requirements*, EPRS: European Parliamentary Research Service, 2021.
19 T. Akçay, M. Häringer, K. Pfeifer, J. Anhalt, J. R. Binder, S. Dsoke, D. Kramer and R. Mönig, $Na_3V_2(PO_4)_3$ –A Highly Promising Anode and Cathode Material for Sodium-Ion Batteries, *ACS Appl. Energy Mater.*, 2021, **4**, 12688–12695.
20 C. V. Manohar, T. C. Mendes, M. Kar, D. Wang, C. Xiao, M. Forsyth, S. Mitra and D. R. MacFarlane, Ionic liquid electrolytes supporting high energy density in sodium-ion batteries based on sodium vanadium phosphate composites, *Chemical communications (Cambridge, England)*, 2018, **54**, 3500–3503.
21 I. U. Mohsin, L. Schneider, M. Häringer, C. Ziebert, M. Rohde, W. Bauer, H. Ehrenberg and H. J. Seifert, Heat generation and degradation mechanisms studied on Na3V2(PO4)3/C positive electrode material in full pouch / coin cell assembly, *Journal of Power Sources*, 2022, **545**, 231901.
22 Anna Smith, Pirmin Stüble, Lea Leuthner, Andreas Hofmann, Fabian Jeschull, Liuda Mereacre, Potential and Limitations of Research Battery Cell Types for Electrochemical Data Acquisition, *Batteries and Supercaps*, 2023.
23 P. Stüble, M. Müller, T. Bergfeldt, J. R. Binder and A. Hofmann, Cycling Stability of Lithium-Ion Batteries Based on Fe-Ti-Doped LiNi0.5 Mn1.5 O4 Cathodes, Graphite Anodes, and the Cathode-Additive Li3 PO4, *Advanced science (Weinheim, Baden-Wurttemberg, Germany)*, 2023, e2301874.
24 M. J. Aragón, P. Lavela, G. F. Ortiz, R. Alcántara and J. L. Tirado, Insight into the Electrochemical Sodium Insertion of Vanadium Superstoichiometric NASICON Phosphate, *Inorganic chemistry*, 2017, **56**, 11845–11853.
25 T. Li, J. Sun, S. Gao, B. Xiao, J. Cheng, Y. Zhou, X. Sun, F. Jiang, Z. Yan and S. Xiong, Superior Sodium Metal Anodes Enabled by Sodiophilic Carbonized Coconut Framework with 3D Tubular Structure, *Advanced Energy Materials*, 2021, **11**, 2003699.
26 M. Liu, J. Zhang, S. Guo, B. Wang, Y. Shen, X. Ai, H. Yang and J. Qian, Chemically Presodiated Hard Carbon Anodes with Enhanced Initial Coulombic Efficiencies for High-Energy Sodium Ion Batteries, *ACS applied materials & interfaces*, 2020, **12**, 17620–17627.
27 L. Zhao, H. Zhao, J. Wang, Y. Zhang, Z. Li, Z. Du, K. Świerczek and Y. Hou, Micro/Nano Na3V2(PO4)3/N-Doped Carbon Composites with a Hierarchical Porous Structure for High-Rate Pouch-Type Sodium-Ion Full-Cell Performance, *ACS applied materials & interfaces*, 2021, **13**, 8445–8454.

28 K. Subramanyan, M. Akshay, Y.-S. Lee and V. Aravindan, Na-Ion Battery with Graphite Anode and Na 3 V 2 (PO 4) 3 Cathode via Solvent-Co-Intercalation Process, *Adv Materials Technologies*, 2022, **7**, 2200399.
29 X. Yin, Y. Zhao, X. Wang, X. Feng, Z. Lu, Y. Li, H. Long, J. Wang, J. Ning and J. Zhang, Modulating the Graphitic Domains of Hard Carbons Derived from Mixed Pitch and Resin to Achieve High Rate and Stable Sodium Storage, *Small (Weinheim an der Bergstrasse, Germany)*, 2022, **18**, e2105568.
30 J. Zhang, J. Gai, K. Song and W. Chen, Advances in electrode/electrolyte interphase for sodium-ion batteries from half cells to full cells, *Cell Reports Physical Science*, 2022, **3**, 100868.
31 X. Jiang, X. Liu, Z. Zeng, L. Xiao, X. Ai, H. Yang and Y. Cao, A Bifunctional Fluorophosphate Electrolyte for Safer Sodium-Ion Batteries, *iScience*, 2018, **10**, 114–122.
32 B. Xiao, F. A. Soto, M. Gu, K. S. Han, J. Song, H. Wang, M. H. Engelhard, V. Murugesan, K. T. Mueller, D. Reed, V. L. Sprenkle, P. B. Balbuena and X. Li, Lithium-Pretreated Hard Carbon as High-Performance Sodium-Ion Battery Anodes, *Adv. Energy Mater.*, 2018, **8**, 1801441.
33 W. Zhang, F. Zeng, H. Huang, Y. Yu, M. Xu, L. Xing and W. Li, Enhanced interphasial stability of hard carbon for sodium-ion battery via film-forming electrolyte additive, *Nano Res.*, 2023, **16**, 3823–3831.
34 J. Klemens, L. Schneider, E. C. Herbst, N. Bohn, M. Müller, W. Bauer, P. Scharfer and W. Schabel, Drying of NCM Cathode Electrodes with Porous, Nanostructured Particles Versus Compact Solid Particles: Comparative Study of Binder Migration as a Function of Drying Conditions, *Energy Tech*, 2022, **10**, 2100985.
35 J. Klemens, D. Burger, L. Schneider, S. Spiegel, M. Müller, N. Bohn, W. Bauer, H. Ehrenberg, P. Scharfer and W. Schabel, Drying of Compact and Porous NCM Cathode Electrodes in Different Multilayer Architectures: Influence of Layer Configuration and Drying Rate on Electrode Properties, *Energy Tech*, 2023. DOI: 10.1002/ente.202300267.
36 J. Klemens, L. Schneider, D. Burger, N. Zimmerer, M. Müller, W. Bauer, H. Ehrenberg, P. Scharfer and W. Schabel, Process and Drying Behavior Toward Higher Drying Rates of Hard Carbon Anodes for Sodium-Ion Batteries with Different Particle Sizes: An Experimental Study in Comparison to Graphite for Lithium-Ion-Batteries, *Energy Tech*, 2023. DOI: 10.1002/ente.202300338.
37 Julian Klemens, Ann-Kathrin Wurba, David Burger, Cedric Müller, Anna Smith, Sebastian Büchele, Marcus Müller, Werner Bauer, Joachim R. Binder, Olatz Leonet, Alberto Blázquez, Elixabeth Ayerbe, Iker Boyano, Helmut Ehrenberg, Jürgen Fleischer, Philip Scharfer, Wilhelm Schabel, Large-scale Electrode Processing of New SIB Materials and Comparison to LIB: From Active Material to Electrode and Cell Design, **chemsuschem**.
38 Cedric Müller, Zhengqi Wang, Andreas Hofmann, Pirmin Stüble, Xinyang Liu-Théato, Julian Klemens, Anna Smith, Influences on electrochemical performance of hard carbon in sodium-ion half-cells, *Batteries and Supercaps*, 2023, submitted.
39 A. Ponrouch, E. Marchante, M. Courty, J.-M. Tarascon and M. R. Palacín, In search of an optimized electrolyte for Na-ion batteries, *Energy Environ. Sci.*, 2012, **5**, 8572.
40 K. Chayambuka, R. Cardinaels, K. L. Gering, L. Raijmakers, G. Mulder, D. L. Danilov and P. H. Notten, An experimental and modeling study of sodium-ion battery electrolytes, *Journal of Power Sources*, 2021, **516**, 230658.
41 A. Hofmann, Z. Wang, S. P. Bautista, M. Weil, F. Müller, R. Löwe, L. Schneider, I. U. Mohsin and T. Hanemann, Comprehensive characterization of propylene carbonate based liquid electrolyte mixtures for sodium-ion cells, *Electrochimica Acta*, 2022, **403**, 139670.
42 G. G. Eshetu, S. Grugeon, H. Kim, S. Jeong, L. Wu, G. Gachot, S. Laruelle, M. Armand and S. Passerini, Comprehensive Insights into the Reactivity of Electrolytes Based on Sodium Ions, *ChemSusChem*, 2016, **9**, 462–471.

43 H. Au, H. Alptekin, A. C. S. Jensen, E. Olsson, C. A. O'Keefe, T. Smith, M. Crespo-Ribadeneyra, T. F. Headen, C. P. Grey, Q. Cai, A. J. Drew and M.-M. Titirici, A revised mechanistic model for sodium insertion in hard carbons, *Energy Environ. Sci.*, 2020, **13**, 3469–3479.

44 J. Fondard, E. Irisarri, C. Courrèges, M. R. Palacin, A. Ponrouch and R. Dedryvère, SEI Composition on Hard Carbon in Na-Ion Batteries After Long Cycling: Influence of Salts (NaPF 6 NaTFSI) and Additives (FEC, DMCF), *J. Electrochem. Soc.*, 2020, **167**, 70526.

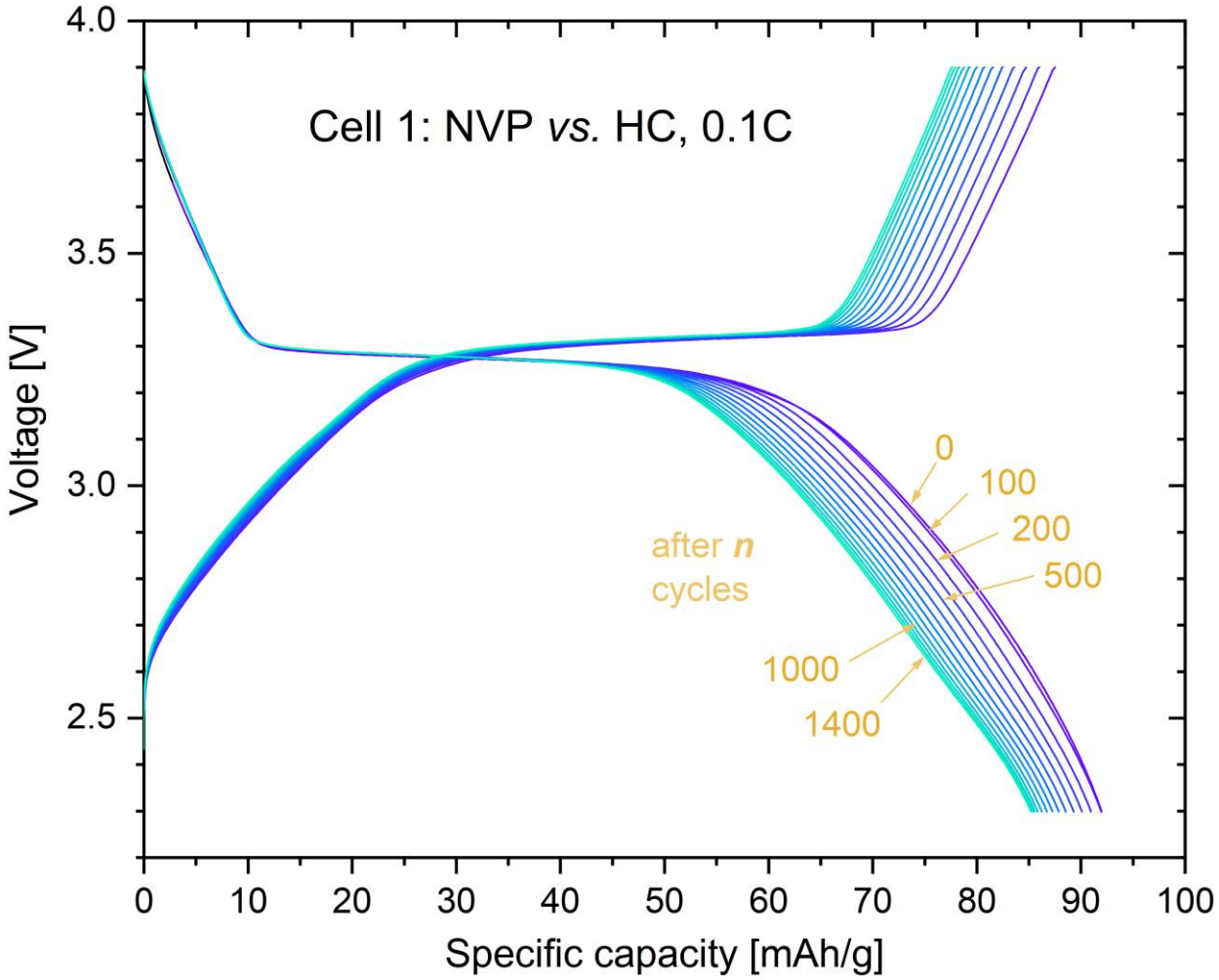

Figure S1: Voltage profiles of the check-up cycles of cell 1 (charge/discharge rages: 0.1 C / 0.1 C). The charging capacity is somewhat reduced compared to the discharge capacity due to the circumstance, that NVP was not fully discharged in the previous 0.5C discharge cycle, leading to coulombic efficiencies of roughly 107 % in the cycles shown.

Table S1: Detailed information about cell building, electrodes and electrolytes in NVP or NVP/C *vs.* HC full cells. "N/A" means that the information was not available in the publication. "?" means that values were given but were not clear to us. "(?)" means that the value given was calculated or estimated by us.

First Author	Year	Ref.	Cell Format	Cathode size	Anode size	Separator	Loading NVP or NVP/C	Loading HC	Balancing	Electrolyte	Vol.	N. of Cycles	Capacity Retention	C-Rate
Aragon	2017	[24]	T-cell	Ø: 0.9 cm	N/A	GF/A	4 mg/cm²	N/A	N/A	1 M NaPF6 in EC/DEC (1:1) + 5 wt % FEC	N/A	150	81,8%	2C
Manohar	2017	[20]	N/A	N/A	N/A	N/A	N/A	N/A	N/A	1 M NaFSI dissolved in N-propyl-N-methyl pyrrolidinium bis(fluoromethanesulfonyl) imide(C3mpyrFSI)	N/A	100	74,0%	C/5
Akcay	2021	[19]	T-cell	Ø: 1.2 cm	Ø: 1.2 cm	GF/B or GF/D	3.34 mg/cm²	N/A	N/A	1 M $NaClO_4$ in EC/DMC (1:1) + 5 wt% of FEC	100 µL	50	66,7%	?
Moshin	2022	[21]	pouch cell	24.5 cm²	N/A	GF/A	1.1 mAh/cm²	1.3 mAh/cm²	1 : 1.18	1 M NaClO4 in EC:DMC:EMC (1:1:1) + 2% FEC	N/A	300	87,9%	C/5
T. Li	2021	[25]	CR2032	Ø: 1.6 cm	Ø: 1.4 cm (?)	Celgard 2400	11 mg/cm²	5 mg/cm²	N/A	1 M $NaPF_6$ in diglyme	50 µL			≈ 0.4C
M. Liu	2020	[26]	N/A	N/A	N/A	glass fiber	N/A	N/A	1 : 1	1 M $NaClO_4$ in PC/EC/DEC (1:1:1)	N/A	550	60,0%	2C
Lina Zhao	2021	[27]	CR2032	N/A	N/A	GF/A	1,5-2,5 mg/cm²	N/A	N/A	1 M $NaClO_4$ in EC/DEC (1:1) + 5% FEC	N/A	200	60,0%	1C
Subramanyan	2022	[28]	CR2016	Ø: 1.4 cm	Ø: 1.4 cm	glass fiber	2.6 mg/cm²	6,5 (RG)	N/A	1 M $NaCF_3SO_3$ in TEGDME	N/A	200	48,0%	≈ C/2 (?)
Yin	2022	[29]	CR2032	Ø: 1.2 cm	Ø: 1.4 cm	GF/D	N/A	N/A	N/A	1 M $NaPF_6$ in diglyme	N/A	450	73,3%	≈ 10 C (?)
Zhang	2023	[33]	CR2025	Ø: 1.2 cm	Ø: 1.4 cm	Celgard 2500	?	?	?	1 M $NaPF_6$ in ED/DEC (1:1) + 1-3wt% PTFSI	80 µL	100	87,0%	1C
Jiang	2018	[31]	CR2016	N/A	N/A	GF/D	3 mg/cm²	1.8 mg/cm²	N/A	0.9 M NaFSI-TFEP	50µL	300	89,0%	≈ 1 C (?)
Xiao	2018	[32]	Coin cell	N/A	N/A	Celgard 3501	N/A	N/A	1:1.5	1M $NaClO_4$ in TEGDME (?) or EC/DMC (1:2) (?)	N/A	50	81,0%	≈ 0.5C (?)
Liu	2022	[10]	CR2032	Ø: 1.0 cm	Ø: 1.0 cm	Celgard 2325	8 mg	3,2-3,3 mg	N/A	1 M $NaPF_6$ in diglyme	40 µL	500	70,2%	1C
This work	2023	--	CR2032	Ø: 1.6 cm	Ø: 1.6 cm	QMA	1.23 mAh/cm²	1.53 mAh/cm²	1:1.22	1 M $NaPF_6$ in EC/PC	110 µL	1000	90,2%	0.5 C

Table S2: Cycling program used for the capacity determination of NVP in the half cell and for the formation of all NVP-vs-HC full-cells. The voltage range in all cases was 2.3 - 3.9 V (NVP vs. working electrode). 1C refers to the theoretical NVP capacity of 117 mAh/g. After the fourth discharge, the cell was charged to 3.5 V (0.05 C).

Step	Number of cycles	Cycles	charge rate	Discharge rate
1	4	1-4	0.05 C	0.05C

Table S3: Cycling program used during the asymmetric rate capability test of the NVP-vs.-HC full-cells 2 and 4 (2.3 - 3.9 V potential of NVP vs. working electrode). For charge after 0.5 C always a CV phase (until I<C/20?) was applied. 1 C refers to the theoretical NVP capacity of 117 mAh/g. After the last discharge cycle, the cell was charged to 3.5 V (0.5C).

Step	Number of Cycles	Cycles number	Charge rate	Discharge rate
1	2	1-2	0.5 C	0.5 C
2	2	3-4	0.5 C	1 C
3	2	5-6	0.5 C	2 C
4	2	7-8	0.5 C	3 C
5	2	9-10	0.5 C	4 C
6	2	11-12	0.5 C	5 C
7	2	13-14	0.5 C	0.5 C

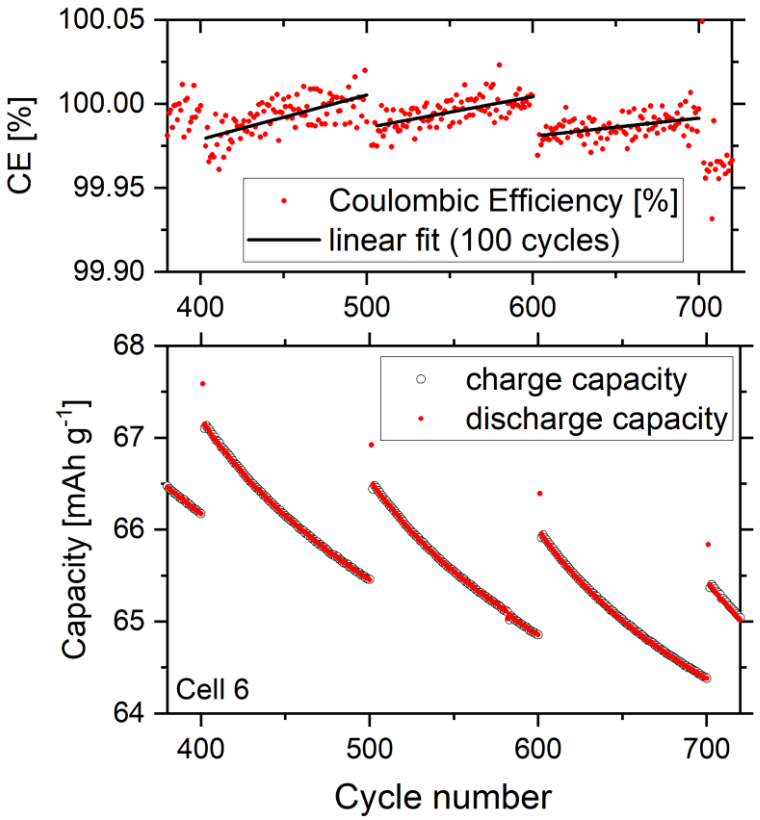

Figure S2: a) Coulombic efficiencies during the cycling stability test of cell 6 (NVP-vs.-HC, 1M $NaPF_6$ in EC:PC with 60 ppm H_2O). Due to the large scattering of the individual CE values, a linear fit for each 100 cycles is plotted (black line). It becomes obvious that after each check-up cycle, the coulombic efficiency is somewhat reduced and then increases over time. The corresponding values for the charge and discharge capacity are shown in subfigure b.